ACS APPLIED MATERIALS & INTERFACES

Research Article

www.acsami.org

Enhanced Performance of Inverted Polymer Solar Cells by Using Poly(ethylene oxide)-Modified ZnO as an Electron Transport Layer

Shuyan Shao,*[,†] Kaibo Zheng,[‡] Tõnu Pullerits,[‡] and Fengling Zhang[†]

[†]Biomolecular and Organic Electronics, Department of Physics, Chemistry and Biology, Linköping University, 58183 Linköping, Sweden

[‡]Department of Chemical Physics, Lund University, Box 124, 22100 Lund, Sweden

ABSTRACT: In this paper, we report enhanced performance of inverted polymer solar cells composed of poly[2,3-bis-(3-octyloxyphenyl)quinoxaline-5,8-diyl-alt-thiophene-2,5-diyl] (TQ1):[6,6]-phenyl-C_{71}-butyric acid methyl ester ($PC_{71}BM$) blends by using poly(ethylene oxide) (PEO)-modified ZnO as an electron transport layer. It is found that PEO modification to the ZnO nanoparticle surface can effectively passivate the surface traps of ZnO, suppress the recombination loss of carriers, reduce the series resistance, and improve the electrical coupling of ZnO/active layer. Consequently, both the short-circuit current (J_{SC}) and the fill factor (FF) of the inverted solar cells are considerably improved. The resulting power conversion efficiency (PCE) is improved to 5.64% as compared to 4.5% of the reference device using a ZnO electron transport layer. Moreover, this approach can also successfully improve the J_{SC} and FF of anther inverted solar cell composed of poly[N-9″-hepta-decanyl-2,7-carbazole-alt-5,5-(4′,7′-dithienyl-2′,1′,3′-benzothiadiazole)] (PCDTBT):$PC_{71}BM$ blends. The PCE of the device based on the PEO-modified ZnO layer is increased to 6.59% from 5.39% of the reference device based on the ZnO layer.

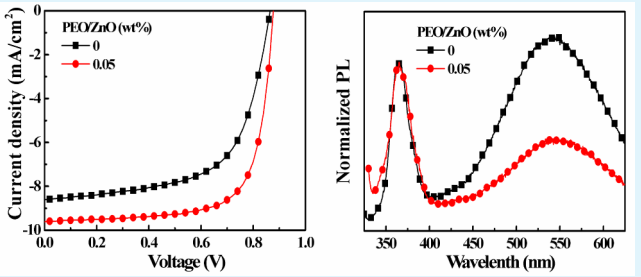

KEYWORDS: *electron transport layer, inverted polymer solar cells, bulk heterojunction, surface modification, ZnO, traps*

1. INTRODCUTION

Polymer solar cells have been a hot research topic due to the motivation for low-cost and green energy. Since the first bulk heterojunction (BHJ) concept proposed by Yu et al., great progress has been made in polymer solar cells by controlling the active morphology and developing new interfacial layers, active materials, and new device structures.[1−14] There are two main device structures. The commonly adopted regular device structure consists of ITO/PEDOT:PSS hole transport layer/active layer/electron transport layer/low work function metal cathode (Al). However, the intrinsic instability of this device structure caused by the low work function metal has been the main concern for many practical applications.[15−19] To overcome this problem, the inverted device structure with a reversed layer sequence, that is, ITO/electron transport layer/active layer/hole transport layer/high work function metal (Ag), has been developed. As compared to the regular device structure, the inverted structure can be fabricated by large-scale and low-cost roll-to-roll printing due to a vacuum-free evaporation process.[20−23] In addition, the inverted device structure has a potentially longer lifetime by using a more ambient stable and higher work function metal as the top anode.[24,25] One of the key factors limiting the performance of the inverted device structure is the electron transport layer. This layer should satisfy several criteria, such as high transparency, high mobility, and high electron affinity energy, to efficiently collect the electrons. Solution-processed ZnO and TiOx have all of these properties and are air stable. Therefore, they are most commonly used as the electron transport layer in inverted solar cells.[26−30] The easy synthesis process and low crystalline temperature of ZnO nanoparticles make them a more attractive candidate for use in polymer solar cells. The major concern with ZnO nanoparticles lies in their surface defects due to their high surface-to-volume ratio. The defects trap electrons, render large series resistance (R_S), and lead to poor electronic coupling with an active layer and severe back charge recombination.[29−32] Coating a thin self-assembled layer, such as carboxylic acid-functionlized fullerene, conjugated polyelectrolyte, or ruthenium dye molecules, on top of the ZnO layer can restrain the surface traps to some extent, which improved electronic coupling of the ZnO/organic layer and consequently improved the short-circuit current density (J_{SC}) and fill factor (FF) of the device.[29−31] The problem with this strategy is that the traps left in the bulk of the ZnO film still prohibit the electron transport due to the voids between ZnO nanoparticles. From an industrial point of view, this strategy is a big challenge for large-area roll-to-roll printing, because the thin self-assembled layer involves only monolayers or a few layers of molecules. Therefore, a simple single-step film-forming process of the electron transport layer is preferred as compared to the

Received: October 21, 2012
Accepted: December 28, 2012
Published: December 28, 2012

complicated two-step film-forming process. Liu et al. recently used amorphous TiOx to fill in the voids between ZnO nanoparticles, passivating the traps in the surface as well as in the bulk of ZnO film.[32] Further efforts need to be paid to the exploration of a new strategy to fabricate simple and low-cost electron transport layers to apply to the large-area roll-to-roll printing technology.

Herein, we developed a generally applicable electron transport layer by poly(ethylene oxide) (PEO) modification to the ZnO nanoparticle surface (PEO:ZnO). Both of the inverted polymer solar cells composed of poly[2,3-bis-(3-octyloxyphenyl)quinoxaline-5,8-diyl-alt-thiophene-2,5-diyl] (TQ1):[6,6]-phenyl-C_{71}-butyric acid methyl ester ($PC_{71}BM$) and poly[N-9″-hepta-decanyl-2,7-carbazole-alt-5,5-(4′,7′-di-thienyl-2′,1′,3′-benzothiadiazole)] (PCDTBT):$PC_{71}BM$ blends show considerably improved device performance by using the PEO:ZnO electron transport layer formed by one-step spin-coating technique. PEO is supposed to be coordinated to the surface of the ZnO nanoparticle by sharing the lone electron pair of oxygen in PEO with ZnO. In this case, PEO modification to the ZnO nanoparticle surface can effectively passivate its surface traps, suppress the trap-assisted recombination loss of carriers, reduce the R_S, and improve the electrical coupling of the ZnO/active layer. Consequently, both J_{SC} and FF of the inverted solar cells are considerably improved.

2. EXPERIMENTAL SECTION

2.1. Materials. The polymer donor TQ1 (Mn = 41000, PDI = 2.6) was synthesized following a previous reported method.[33] PCDTBT (M_w = 24000, PDI = 1.8) was purchased from Solarmer Energy Co., and the acceptor $PC_{71}BM$ was from Solenne BV. PEO (M_w = 100000) was purchased from BDH Chemicals Ltd. ZnO was synthesized following the previous procedure by Week et al.[34] Four grams of zinc acetate dihydrate (>99%) was dissolved in 160 mL of methanol at 60 °C under vigorous stirring. Two grams of KOH (>85%) was dissolved in 80 mL of methanol. The KOH solution was dropped into the zinc acetate dihydrate solution in 10 min under vigorous stirring. The solution temperature was held at 60 °C and stirred for 4 h, and then, the heating and stirring were removed to allow particles to precipitate for an additional 12 h. The precipitate was cleaned by centrifugation of the dispersion and washed twice with 50 mL of methanol. The washed ZnO nanoparticles were dissolved in chlorobenzene (CB) to form a 20 mg/mL ZnO CB solution. Surface modification of ZnO by PEO was achieved by adding the desired concentration of PEO into the ZnO solution.

2.2. Fabrication of Inverted Polymer Solar Cells. ITO-coated glass substrates were first cleaned with detergent and deionized water and then dried by nitrogen flow. A 30 nm thick ZnO layer or PEO:ZnO layer was spin coated on top of the ITO substrates as the electron transport layer. A solution containing a mixture of TQ1:$PC_{71}BM$ (9 mg/mL:27 mg/mL) or PCDTBT:$PC_{71}BM$ (7 mg/mL: 28 mg/mL) in dichlorobenzene was spin-cast on top of the electron transport layer to produce a 120 nm thick or 80 nm thick active layer. Finally, a bilayer structure of MoO_3 (7 nm)/Ag (80 nm) was deposited atop the active layer by thermal evaporation in a vacuum of 4×10^{-6} Torr to complete the device fabrication. The cell active area was 5 mm^2, which was defined by the overlapping area of the ITO and Ag electrodes. The solar cells were characterized with a Keithley 2400 source meter under simulated AM 1.5 solar illumination (100 mW cm^{-2}), calibrated with a silicon solar reference cell (SRC-1000-RTD). External quantum efficiency (EQE) of the devices was collected by a Keithley 485 picoammeter under illumination of monochromatic light at short-circuit conditions.

2.3. Other Characterization. Atomic force microscopy (AFM) images were recorded on a Dimension 3100 system (Digital Instruments/Veeco) in tapping mode. Steady-state emission spectra (PL) of the ZnO samples were measured using a SPEX 1681 automated spectrofluorometer. The excitation wavelength was 330 nm.

3. RESULTS AND DISCUSSION

Figure 1a–c shows the chemical structures of electron donor TQ1, electron acceptor $PC_{71}BM$, and surface modifier PEO,

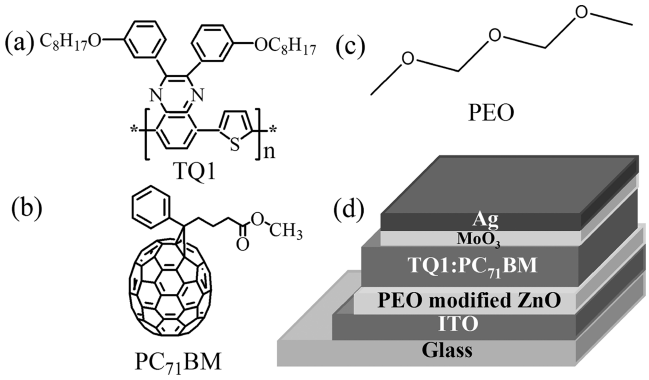

Figure 1. Chemical structures of (a) TQ1, (b) $PC_{71}BM$, (c) PEO, and (d) the device structure used in this work.

respectively. Figure 1d shows the inverted device structure used in this work, where the high-work-function molybdenum trioxide (MoO_3) was deposited on top of the BHJ layer as the hole transport layer and various PEO-modified ZnO layers as the underneath electron transport layer. The focus of the present work is the effect of PEO modification to ZnO nanoparticle on the properties of the ZnO interlayer and the performance of PSCs.

The illuminated current–voltage (*J-V*) characteristics under AM 1.5G irradiation (100 mW cm^{-2}) of TQ1:$PC_{71}BM$ solar cells using various PEO:ZnO electron transport layers are shown in Figure 2a. The corresponding device parameters are listed in Table 1. As can be seen, the reference device using ZnO as the cathode buffer layer shows an open circuit voltage (V_{OC}) of 0.864 V, a J_{SC} of 8.69 mA cm^{-2}, a FF of 0.60, and a power conversion efficiency (PCE) of 4.50%. The device performance was considerably improved when PEO-modified ZnO was used as the electron transport layer. The optimum device was achieved when using 0.05% PEO-modified ZnO (weight ratio of PEO to ZnO) as the electron transport layer, which displays a V_{OC} of 0.877 V, a J_{SC} of 9.60 mA cm^{-2}, a FF of 0.67, and a PCE of 5.64%. However, as the PEO loading was further increased, the device performance decreased. When the PEO content was increased up to 1%, the device showed a decreased J_{SC} of 7.70 mA cm^{-2} and a reduced FF of 0.55, giving a final PCE of 3.68%. With all of the PEO:ZnO layers showing similar transmittance (the data are not shown here), the optical improvement can be excluded as the main contributor to the enhanced J_{SC}. To disclose the origin of performance enhancement, the R_S and shunt resistance (R_P) of the polymer solar cells were extracted from the illuminated *J-V* characteristics and also summarized in Table 1. The R_S reflects the ohmic loss in the entire device structure including contact resistance at the interface and the bulk resistance of the interfacial layers and the active material. The R_P reflects the loss of charge carriers due to the current leakage pathways and recombination of charges in the bulk or at the interface. The reference device shows a R_S of 22 Ω cm^2 and a shunt resistance of 0.9 kΩ cm^2, respectively. The device using 0.05% PEO-modified ZnO as the electron

dx.doi.org/10.1021/am302408w | ACS Appl. Mater. Interfaces 2013, 5, 380–385

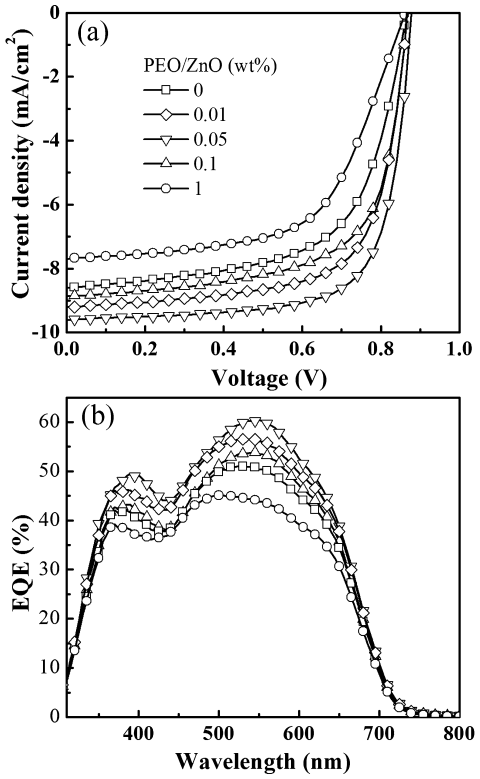

Figure 2. (a) Illuminated *J-V* characteristics and (b) EQE data of devices based on TQ1:$PC_{71}BM$ blends using PEO-modified ZnO cathode buffer layers.

Table 1. Performance Parameters of the Devices Based on TQ1:$PC_{71}BM$ Blends Using PEO-Modified ZnO Electron Transport Layers

devices	V_{OC} (V)	J_{SC} (mA cm^{-2})	FF	R_S (Ω cm^2)	R_P (kΩ cm^2)	PCE (%)
ITO/ZnO	0.864	8.69	0.6	22	0.9	4.50
ITO/1% PEO:ZnO	0.869	7.70	0.55	30	1.3	3.68
ITO/0.1% PEO:ZnO	0.876	8.87	0.64	10	1.5	4.97
ITO/0.05% PEO:ZnO	0.877	9.6	0.67	8.1	2.17	5.64
ITO/0.01% PEO:ZnO	0.872	9.2	0.65	8.6	1.6	5.21

transport layer shows the smallest R_S of 8 Ω cm^2 and the highest R_P of 2.17 kΩ cm^2. The reduced R_S is favorable for charge collection, and the increased R_P indicates reduced leakage current as well as restrained recombination loss of carriers, which explains the improved FF and J_{SC}. When the PEO content is increased up to 1%, the R_S of the device is increased to 30 Ω cm^2, which renders a large energy barrier for charge collection. In this case, many carriers recombine before they are collected at the electrodes. Therefore, the small FF and J_{SC} can be expected when charge collection is inefficient due to the presence of large R_S. Figure 2b shows the EQE data of the devices. It shows a similar tendency as that of J_{SC}, further confirming the improved photoelectron conversion efficiency.

It has been well documented in the literature that the surface states of ZnO nanoparticle are very sensitive to the surface adsorbates due to the its high surface-to-volume ratio.[35,36] To investigate the effect of PEO modification on surface defects of ZnO nanoparticles, PL spectra were recorded for various PEO-modified ZnO films as shown in Figure 3. As can be seen, two emission peaks were observed. The narrow emission band at

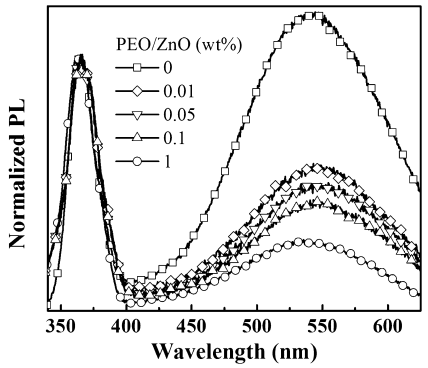

Figure 3. PL spectra of PEO-modified ZnO films on top of glass substrate.

365 nm (3.4 eV) is attributed to radiative annihilation of excitons (exciton emission), while the intense broad emission around 550 nm (2.25 eV) is assigned to the trap emission.[35,36] It shows clearly that the defect emission is considerably restrained by surface modification of ZnO by PEO, indicating reduced surface traps of ZnO after PEO surface modification. It is proposed that PEO species coordinate with ZnO by sharing a lone electron pair of oxygen in the PEO backbone, which effectively passivates the surface traps of ZnO. The fill-up of surface electron traps of ZnO favors the improvement in the conductivity of ZnO interlayer, leading to the reduced R_S of devices. Moreover, the reduction of traps can decrease the possibility of trap-assisted interfacial recombination of carriers and consequently increase the R_P of devices. Both reasons contribute to the improved J_{SC} and FF for the PEO-modified ZnO-based devices when the PEO loading is less than 1%.

Figure 4 shows the dark *J-V* curves on logarithm scale of the reference device and the device with 0.05% PEO-modified ZnO electron transport layer and the schematics of charge transfer processes in devices at small forward bias. As can be seen in Figure 4a, the leakage current of the device with PEO:ZnO electron transport layer is considerably restrained, and the rectification ratio of the device with 0.05% PEO-modified device is considerably increased. The corresponding mechanism was proposed in Figure 4b, taking the small forward bias case as the example. At small forward bias, the electrons are injected into the conductive band (CB) of ZnO layer from the ITO side and further transferred to the lowest unoccupied molecular orbit (LUMO) of the acceptor. The holes are injected to the valence band (VB) of MoO_3 layer and then transferred to the highest occupied molecular orbit (HOMO) of the donor. Although the hole-transfer pathway from the HOMO of the donor to the VB of ZnO layer is energetically forbidden, the holes can recombine with the electrons in traps of the ZnO layer, forming forward leakage current. Because the number of electron traps in ZnO nanoparticles can be substantially decreased by PEO modification, it is expected that the leakage current is reduced for PEO-modified ZnO-based devices with respect to unmodified cases. These results further confirm that the PEO species can effectively passivate the traps of ZnO nanoparticle surface, leading to improved electrical coupling with the active layer.

To gain further insight into the variation in the device performance, information about the surface morphology of

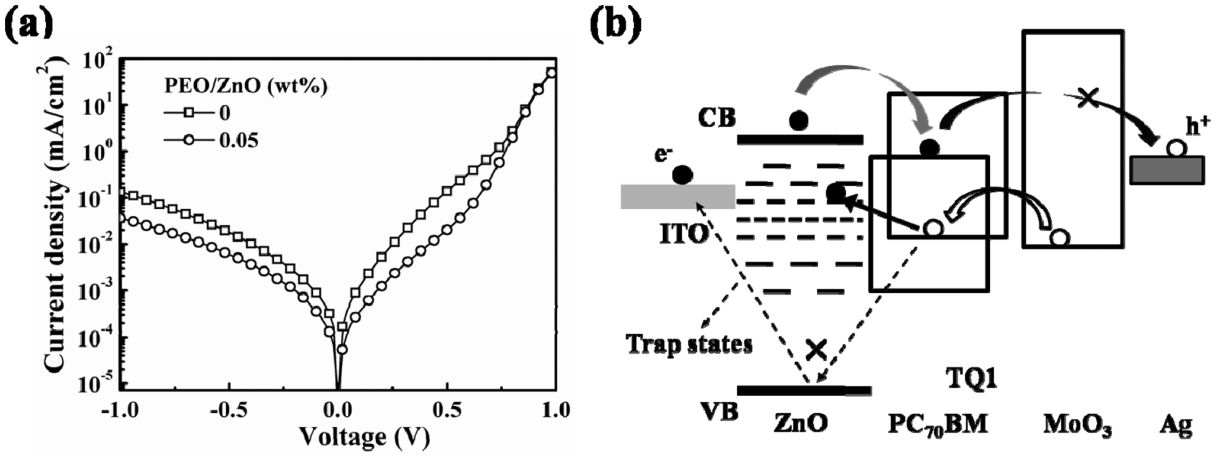

Figure 4. (a) Dark *J-V* curves of the devices using ZnO and 0.05% PEO-modified ZnO electron transport layers. (b) Schematics of charge transfer processes in devices at small forward bias.

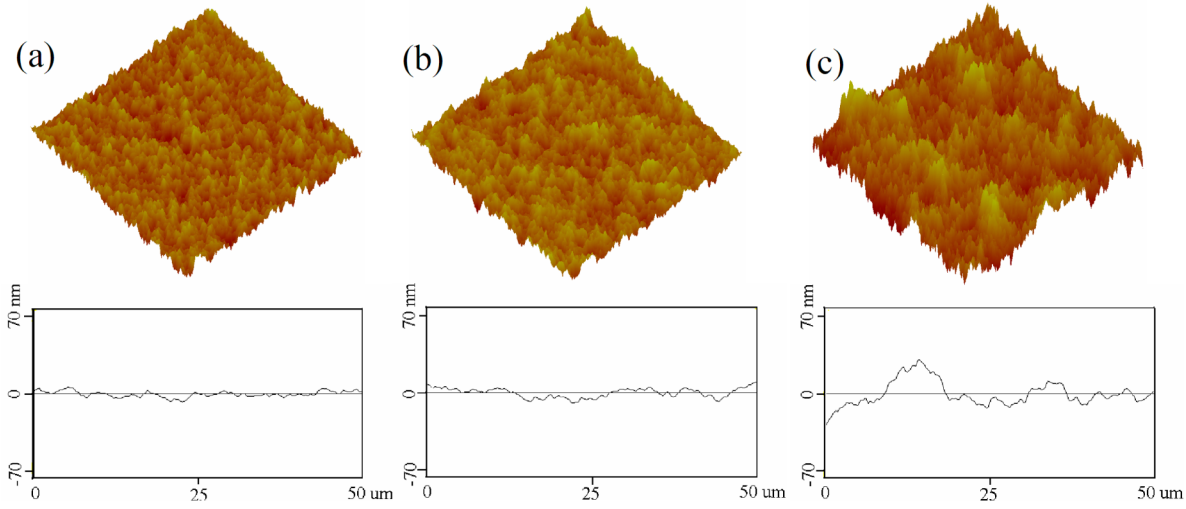

Figure 5. Topography images of (a) ZnO, (b) 0.05% PEO-modified ZnO, and (c) 1% PEO-modified ZnO.

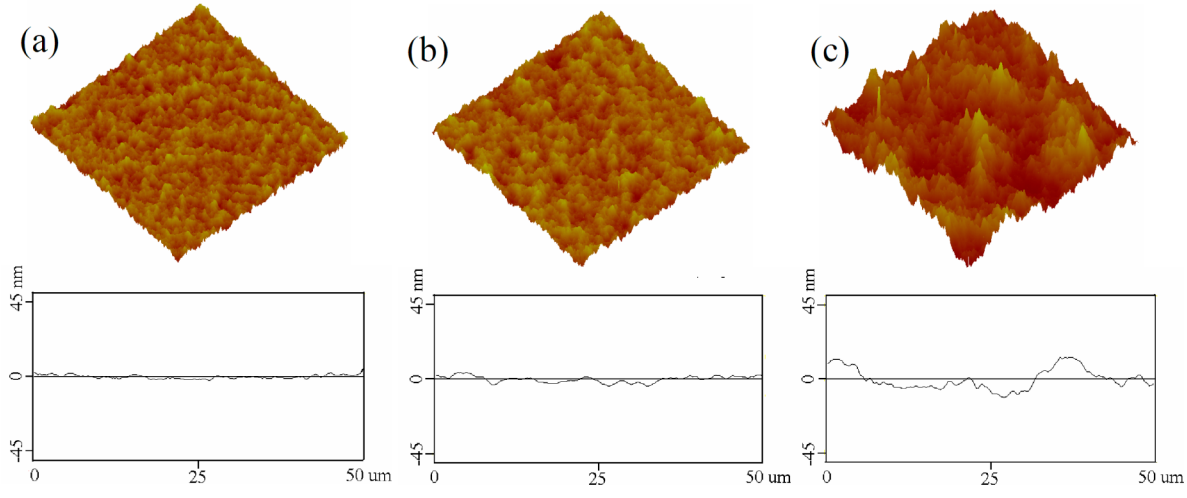

Figure 6. Topography images of TQ1:PC$_{71}$BM films on top of (a) ZnO, (b) 0.05% PEO-modified ZnO, and (c) 1% PEO-modified ZnO.

PEO:ZnO layers and the active layers is necessary. First, the surface morphology of PEO-modified ZnO layer is investigated by AFM. As can be seen from Figure 5, the 0.05% PEO-modified ZnO film shows a similar surface morphology to that of the pristine ZnO film. However, when the PEO content is further increased up to 1%, a very rough surface of ZnO forms. The root-mean-square (RMS) roughness is increased to 34 nm from 6 nm of the pristine ZnO film. The variation in surface morphology may be caused by the change in the surface property of ZnO nanoparticles after PEO modification. The

dx.doi.org/10.1021/am302408w | *ACS Appl. Mater. Interfaces* 2013, 5, 380−385

water-soluble PEO molecules make the surface of the ZnO nanoparticle more hydrophilic and incompatible with nonpolar chlorobenzene solvent, leading to larger ZnO aggregates in solution and solid films. Water contact angle tests were further performed for pristine ZnO and 1% PEO-modified ZnO. The water contact angle is decreased from 30° of the pristine ZnO film to 20° of the 1% PEO-modified ZnO film. These results confirm the more hydrophilic property of PEO-modified ZnO surface. The large ZnO aggregates render not only large bulk resistance of ZnO film but also large interfacial contact resistance with active layer, leading to the decrease in the device performance.

The surface morphology of TQ1:$PC_{71}BM$ is further investigated by AFM as shown in Figure 6. Likewise, a similar surface morphology of the TQ1:$PC_{71}BM$ film on top of the 0.05% PEO-modified ZnO film as that on top of the pristine ZnO is observed. When the PEO content is increased up to 1%, the surface of the TQ1:$PC_{71}BM$ film becomes very rough. The RMS value is increased to 20 nm from 2 nm of the active layer on top of the pristine ZnO. The rougher active layer is unfavorable for the device performance. It renders a large contact resistance between the active layer and the cathode. Moreover, the rough PEO:ZnO layer penetrates into the TQ1:$PC_{71}BM$ active layer, extending the contact area between hydrophilic PEO:ZnO and the active layer. Previous reports have proved that the variation in surface property of interfacial layer can induce changes in the active morphology based on the fact that PCBM is more hydrophilic than that of the polymer.[37,38] The hydrophilic underneath PEO:ZnO layer may induce $PC_{71}BM$ to demix out of TQ1 matrix, form larger phase separation domains, and consequently reduce the exciton dissociation efficiency. As is known, emission from a polymer donor decreases as charge transfer from a polymer donor to PCBM electron acceptor (exciton dissociation). Therefore, the PL measurement is a useful tool to detect the exciton dissociation efficiency by evaluating PL quenching of the polymer. Here, PL spectra were recorded for the TQ1:$PC_{71}BM$ films on top of various PEO-modified ZnO layers as shown in Figure 7. As can be seen, the intensity of emission from TQ1

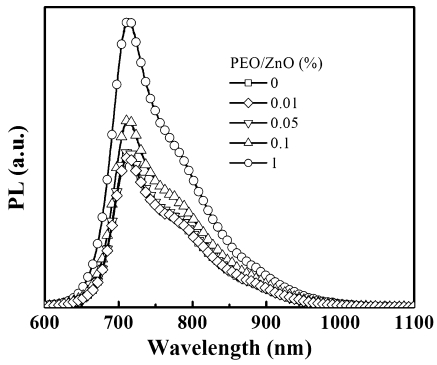

Figure 7. PL spectra of TQ1:$PC_{71}BM$ film on top of PEO-modified ZnO films.

was similar when the PEO content is lower than 0.05%, indicating similar exciton dissociation efficiency. When the PEO content is higher than 0.05%, the PL intensity of TQ1 is considerably increased, which indicates less efficient exciton dissociation. The exciton dissociation efficiency is determined by the interfacial area between the polymer donor and the electron acceptor because of the limited exciton diffusion length. It verifies the reduced interfacial area between the polymer donor and the electron acceptor $PC_{71}BM$. Thus, the performance variation of the devices using various PEO-modified ZnO electron transport layers can be explained. When the PEO content is lower than 1%, the reduced surface traps of ZnO reduces R_S and restrains the trap-assisted recombination. Therefore, it favors electron transport and improves electron coupling with the active layer. All of these factors contribute to the improved FF and J_{SC} of the 0.05% PEO-modified device. However, as the PEO content is increased up to 1%, the reduced exciton dissociation efficiency and increased contact resistance lead to reduced device performance.

It is worth mentioning that this approach was also successfully applied in another well-studied material system (PCDTBT:$PC_{71}BM$ blends). The Figure 8a inset shows the

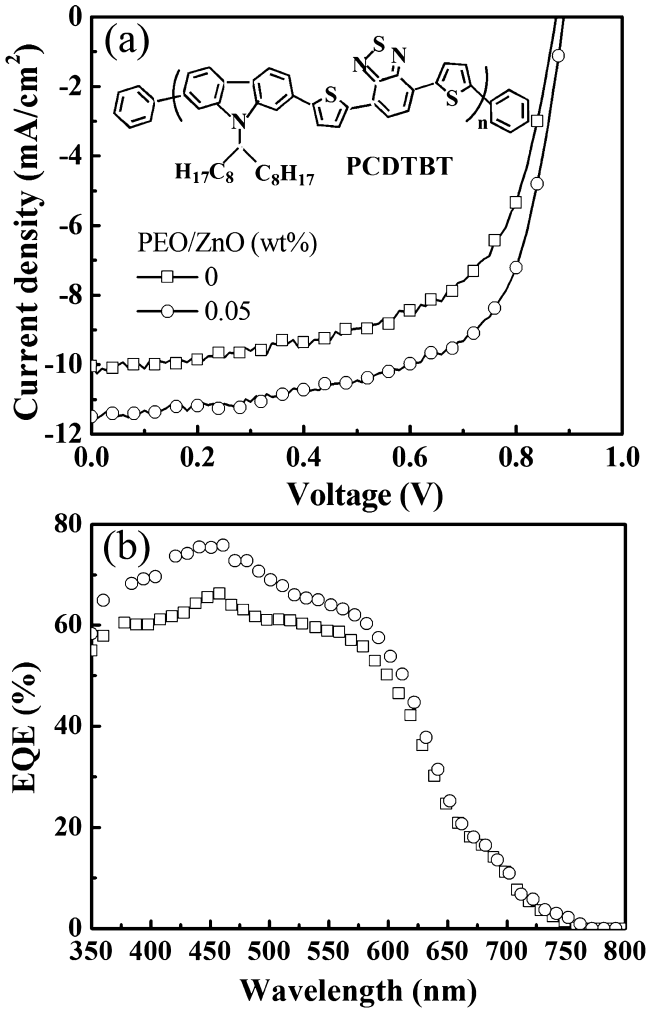

Figure 8. (a) Illuminated *J-V* characteristics and (b) EQE spectra of devices based on PCDTBT:$PC_{71}BM$ blends using PEO-modified ZnO cathode buffer layers (the inset shows the chemical structure of PCDTBT).

chemical structure of PCDTBT. Figure 8a shows the illuminated *J-V* curves of devices using ZnO and 0.05% PEO-modified ZnO cathode buffer layers. Similar variation in the performance of PCDTBT-based device was observed as previous TQ1-based devices. The device using a 0.05% PEO-modified ZnO layer shows considerably improved J_{SC} of 11.4 mA cm^{-2} and FF of 0.65 as compared to the reference device,

dx.doi.org/10.1021/am302408w | ACS Appl. Mater. Interfaces 2013, 5, 380−385

which shows a J_{SC} of 10.2 mA cm^{-2} and a FF of 0.6. Consequently, the device using a 0.05% PEO-modified ZnO layer shows considerably improved PCE of 6.59% as compared to 5.39% of the device with the ZnO layer. The EQE spectra shown in Figure 8b confirm the improved J_{SC} of the device-based PEO-modified ZnO layer. These results demonstrate a generally applicable approach to improve the performance of the inverted polymer solar cells.

4. CONCLUSION

In conclusion, we studied the effects of various PEO-modified ZnO electron transport layers on the performance of inverted polymer solar cells. It was demonstrated that PEO modification to the ZnO nanoparticle surface can effectively passivate its surface traps, suppress the recombination loss of carriers, reduce the series resistance, and improve the electrical coupling of the ZnO/active layer. Consequently, both J_{SC} and FF of the inverted solar cells are considerably improved. For TQ1:$PC_{71}BM$ and PCDTBT:$PC_{71}BM$ based inverted solar cells, the PCEs are significantly improved from the original 4.5 and 5.39% to 5.64 and 6.59%, respectively. These results indicate a generally applicable electron transport layer for ambient stable and high-efficiency inverted polymer solar cells.

AUTHOR INFORMATION

Corresponding Author

*E-mail: sshuyan@126.com.

Notes

The authors declare no competing financial interest.

ACKNOWLEDGMENTS

We are grateful to the Swedish energy agency (Energimyndigheten), the Swedish Research Council (VR), the Knut, Alice Wallenberg Foundation, Crafoord foundation, and VINNOVA for the financial support.

REFERENCES

(1) Yu, G.; Gao, J.; Hummelen, J. C.; Wudl, F.; Heeger, A. J. *Science* **1995**, *270*, 1789−1791.
(2) Padinger, F.; Rittberger, R. S.; Sariciftci, N. S. *Adv. Funct. Mater.* **2003**, *13*, 85−88.
(3) Li, G.; Shrotriya, V.; Huang, J.; Yao, Y.; Moriarty, T.; Emery, K.; Yang, Y. *Nat. Mater.* **2005**, *4*, 864−868.
(4) Li, G.; Yao, Y.; Yang, H.; Shrotriya, V.; Yang, G.; Yang, Y. *Adv. Funct. Mater.* **2007**, *17*, 1636−1644.
(5) Wang, W. L.; Wu, H. B.; Yang, C. Y.; Luo, C.; Zhang, Y.; Chen, J. W.; Cao, Y. *Appl. Phys. Lett.* **2007**, *90*, 183512−1−3.
(6) Lee, J. K.; Ma, W. L.; Brabec, C. J.; Yuen, J.; Moon, J. S.; Kim, J. Y.; Lee, K.; Bazan, G. C.; Heeger, A. J. *J. Am. Chem. Soc.* **2008**, *130*, 3619−3623.
(7) Zhang, F.; Ceder, M.; Inganäs, O. *Adv. Mater.* **2007**, *19*, 1835−1838.
(8) He, Z.; Zhong, C.; Su, S.; Xu, M.; Wu, H.; Cao, Y. *Nat. Photon.* **2012**, *6*, 593−597.
(9) Chen, H.-Y.; Hou, J.; Zhang, S.; Liang, Y.; Yang, G.; Yang, Y.; Yu, L.; Wu, Y.; Li, G. *Nat. Photon.* **2009**, *3*, 649−653.
(10) Chang, C.-Y.; Wu, C.-E.; Chen, S.-Y.; Cui, C.; Cheng, Y.-J.; Hsu, C.-S.; Wang, Y.-L.; Li, Y. *Angew. Chem., Int. Ed.* **2011**, *123*, 9558−9562.
(11) Li, F.; Zhou, Y.; Zhang, F.; Liu, X.; Zhan, Y.; Fahlman, M. *Chem. Mater.* **2009**, *21*, 2798−2802.
(12) Li, W.; Qin, R.; Zhou, Y.; Andersson, M.; Li, F.; Zhang, C.; Li, B.; Liu, Z.; Bo, Z.; Zhang, F. *Polymer* **2010**, *51*, 3031−3038.
(13) Zhen, H.; Li, K.; Huang, Z.; Zheng, T.; Wu, R.; Li, G.; Liu, X.; Zhang, F. *Appl. Phys. Lett.* **2012**, *100*, 213901−1−3.
(14) Zhou, Y.; Li, F.; Barrau, S.; Tian, W.; Inganäs, O.; Zhang, F. *Sol. Energy Mater. Sol. Cells* **2009**, *93*, 497−500.
(15) Jin, H.; Tao, C.; Velusamy, M.; Aljada, M.; Zhang, Y.; Hambsch, M.; Burn, P. L.; Meredith, P. *Adv. Mater.* **2012**, *24*, 2572−2577.
(16) Krebs, F. C.; Gevorgyan, S. A.; Alstrup, J. *J. Mater. Chem.* **2009**, *19*, 5442−5451.
(17) Norrman, K.; Gevorgyan, S. A.; Krebs, F. C. *ACS Appl. Mater. Interfaces* **2009**, *1*, 102−112.
(18) Hau, S. K.; Yip, H.-L.; Acton, O.; Baek, N. S.; Ma, H.; Jen, A. K.-Y. *J. Mater. Chem.* **2008**, *18*, 5113−5119.
(19) Voroshazi, E.; Verreet, B.; Buri, A.; Müller, R.; Nuzzeo, D. D.; Heremans, P. *Org. Electron.* **2011**, *12*, 736−744.
(20) Dupont, S. R.; Oliver, M.; Krebs, F. C.; Dauskardt, R. H. *Sol. Energy Mater. Sol. Cells* **2012**, *97*, 171−175.
(21) Søndergaard, R.; Hösel, M.; Angmo, D.; Larsen-Olsen, T. T.; Krebs, F. C. *Mater. Today* **2012**, *15*, 36−49.
(22) Krebs, F. C.; Fyenbo, J.; Tanenbaum, D. M.; Gevorgyan, S. A.; Andriessen, R.; Remoortere, B.; Galagan, Y.; Jørgensen, M. *Energy Environ. Sci.* **2011**, *4*, 4116−4123.
(23) Krebs, F. C.; Nielsen, T. D.; Fyenbo, J.; Wadstrøm, M.; Pedersen, M. S. *Energy Environ. Sci.* **2010**, *3*, 512−525.
(24) Lloyd, M. T.; Peters, C. H.; Garcia, A.; Kauvar, I. V.; Berry, J. J.; Reese, M. O.; McGehee, M. D.; Ginley, D. S.; Olson, D. C. *Sol. Energy Mater. Sol. Cells* **2011**, *95*, 1382−1387.
(25) Lloyd, M. T.; Olson, D. C.; Lu, P.; Fang, E.; Moore, D. L.; White, M. S.; Reese, M. O.; Ginley, D. S.; Hsu, J. W. P. *J. Mater. Chem.* **2009**, *19*, 7638−7642.
(26) Hau, S. K.; Yip, H.-L.; Baek, N. S.; Zou, J.; Malley, K. O.; Jen, A. K.-Y. *Appl. Phys. Lett.* **2008**, *92*, 253301-1-3.
(27) White, M. S.; Olson, D. C.; Shaheen, S. E.; Kopidakis, N.; Ginley, D. S. *Appl. Phys. Lett.* **2006**, *89*, 143517-1-3.
(28) Steim, R.; Choulis, S. A.; Schilinsky, P.; Brabec, C. J. *Appl. Phys. Lett.* **2008**, *92*, 093303-1-3.
(29) Hau, S. K.; Yip, H.-L.; Ma, H.; Jen, A. K.-Y. *Appl. Phys. Lett.* **2008**, *93*, 233304-1-3.
(30) Seo, J. H.; Gutacker, A.; Sun, Y.; Wu, H.; Huang, F.; Cao, Y.; Scherf, U.; Heeger, A. J.; Bazan, G. C. *J. Am. Chem. Soc.* **2011**, *133*, 8416−8419.
(31) Gadisa, A.; Liu, Y.; Samulski, E. T.; Lopez, R. *Appl. Phys. Lett.* **2012**, *100*, 253903.
(32) Liu, J.; Shao, S.; Meng, B.; Fang, G.; Xie, Z.; Wang, L. *Appl. Phys. Lett.* **2012**, *100*, 213906-1-3.
(33) Wang, E.; Tao, L.; Wang, Z.; Hellström, S.; Zhang, F.; Inganäs, O.; Andersson, M. R. *Adv. Mater.* **2010**, *22*, 5240−5244.
(34) Beek, W. J. E.; Wienk, M. M.; Janssen, A. J. R. *Adv. Funct. Mater.* **2006**, *16*, 1112−1116.
(35) Dijken, A.; Meulenkamp, E. A.; Vanmaekelbergh, D.; Meijerink, A. *J. Phys. Chem. B* **2000**, *104*, 4355−4360.
(36) Dijken, A.; Meulenkamp, E. A.; Vanmaekelbergh, D.; Meijerink, A. *J. Phys. Chem. B* **2000**, *104*, 1715−1723.
(37) Shao, S.; Liu, L.; Zhang, J.; Zhang, B.; Xie, Z.; Geng, Y.; Wang, L. *ACS Appl. Mater. Interfaces* **2012**, *4*, 5704−5710.
(38) Xu, Z.; Chen, L.-M.; Yang, G.; Huang, C.-H.; Hou, J.; Wu, Y.; Li, G.; Hsu, C.-S.; Yang, Y. *Adv. Funct. Mater.* **2009**, *19*, 1227−1234.